FED-Vol. 226, Cavitation and Gas-Liquid Flow
in Fluid Machinery Devices
ASME 1995

THE NOISE GENERATED BY THE COLLAPSE OF A CLOUD OF CAVITATION BUBBLES

Y.-C. Wang and C.E. Brennen

California Institute of Technology,
Pasadena, California 91125

ABSTRACT

The focus of this paper is the numerical simulation of the dynamics and acoustics of a cloud of cavitating bubbles. The prototypical problem solved considers a finite cloud of nuclei that is exposed to a decrease in the ambient pressure which causes the cloud to cavitate. A subsequent pressure recovery then causes the cloud to collapse. This is typical of the perturbation experienced by a bubble cloud as it passes a headform or the blade of a ship propeller. The simulations employ the fully non-linear, non-barotropic, homogeneous flow equations coupled with the Rayleigh-Plesset dynamics for individual bubbles. This set of equations is solved numerically by an integral method. The computational results confirm the early speculation of Mørch and his co-workers (Mørch 1980 & 1981, Hanson *et al.* 1981) that an inwardly propagating shock wave may be formed in the collapse of a cavitating cloud. The structure of the shock is found to be similar to that of the steady planar shocks analyzed by Noordij and van Wijngaarden (1974). The shock wave grows rapidly not only because of the geometric effect of an inwardly propagating spherical shock but also because of the coupling of the single bubble dynamics with the global dynamics of the flow through the pressure and velocity fields (see also Wang and Brennen 1994). The specific circumstances which lead to the formation of such a shock are explored. Moreover, the calculations demonstrate that the acoustic impulse produced by the cloud is significantly enhanced by this shock-focusing process.

Major parameters which affect the dynamics and acoustics of the cloud are found to be the cavitation number, σ, the initial void fraction, α_0, the minimum pressure coefficient of the flow, C_{PMIN}, the natural frequencies of the cloud, and the ratio of the length scale of low pressure perturbation to the initial radius of the cloud, D/A_0, where D can be, for example, the radius of the headform or chord length of the propeller blade. We examine how some of these parameters affect the far field acoustic noise produced by the volumetric acceleration of the cloud. The non-dimensional far-field acoustic impulse produced by the cloud collapse is shown to depend, primarily, on the maximum total volume of the bubbles in the cloud normalized by the length scale of the low pressure perturbation. Also, this maximum total volume decreases quasi-linearly with the increase of the cavitation number. However, the slope of the dependence, in turn, changes with the initial void fraction and other parameters. Non-dimensional power density spectra for the far-field noise are presented and exhibit the f^{-n} behavior, where n is between 0.5 and 2. After several collapse cycles, the cloud begins to oscillate at its natural frequency and contributes harmonic peaks in its spectrum.

Nomenclature

A	Dimensionless radius of the bubble cloud
A_0	Dimensionless radius of the bubble cloud at the undisturbed reference condition
C_P	Pressure coefficient, $(p-p_0)/\frac{1}{2}\rho_L U^2$
$C_{P\infty}$	Pressure coefficient at infinity, $(p_\infty - p_0)/\frac{1}{2}\rho_L U^2$
C_{PMIN}	Minimum pressure coefficient at infinity
D	Length scale of the low pressure perturbation
R	Dimensionless bubble radius
R_0	Initial radius of bubble at undisturbed reference condition
Re	Reynolds number, $\rho_L U R_0/\mu_E$
S	Surface tension of the liquid
U	Reference velocity of the flow
V_{BMAX}	Maximum total volume of bubbles in the cloud
We	Weber number, $\rho_L U^2 R_0/S$
k	Effective polytropic index for the gas inside the bubbles
p	Fluid pressure
p_0	Fluid pressure at undisturbed reference condition
p_a	Dimensionless far-field acoustic pressure produced by the cloud

p_v	Vapor pressure inside the bubble
p_∞	Pressure at infinity
r	Dimensionless Eulerian radial coordinate measured from the center of cloud
r_0	Dimensionless Lagrangian radial coordinate measured from the center of cloud and equal to r at the undisturbed reference condition
t	Dimensionless time
t_G	Dimensionless duration of the low pressure perturbation
u	Dimensionless radial velocity of the fluid
α	Void fraction of the bubbly mixture
α_0	Void fraction of the bubble mixture at the undisturbed reference condition
ρ_L	Density of the liquid
σ	Cavitation number, $(p_0 - p_v)/\frac{1}{2}\rho_L U^2$
η	Dimensionless bubble population per unit liquid volume
μ_E	Effective dynamic viscosity of the liquid

1 Introduction

Experimental studies of cloud cavitation have demonstrated that severe noise and damage potential are associated with the collapse of a cavitating cloud of bubbles (see, for example, Bark and Berlekom 1978, Shen and Peterson 1978, Bark 1985, Franc and Michel 1988, Kubota *et al.* 1989, and Reisman *et al.* 1994). The coherent collapse of a cavitating cloud can be more violent than that of individual bubbles and thus increase the noise and damage potential (Bark and Berlekom 1978, Soyoma *et al.* 1992, and Reisman *et al.* 1994). However, the basic explanation of the enhanced noise and damage potential is still not clear. Most previous theoretical studies of the dynamics of cavitating clouds have been linear or weakly non-linear analyses which have identified the natural frequencies and modes of cloud oscillation (see, for example, d'Agostino and Brennen 1983 & 1989, Kumar and Brennen 1991, 1992, 1993) but have not, as yet, shown how a cloud would behave during the massively non-linear response in a cavitating flow.

Several years ago, Mørch and his co-workers (Mørch 1980 & 1981, Hanson *et al.* 1981) speculated that the collapse of a cloud of bubbles involves the formation and inward propagation of a shock wave and that the geometric focusing of this shock at the center of cloud creates the enhancement of the noise and damage potential associated with cloud collapse. Recently we have employed a continuum mixture model to study the nonlinear growth and collapse of a spherical cloud of bubbles and confirmed that the collapse is accompanied by the formation of such a shock wave which rapidly gains strength (Wang and Brennen 1994). The present paper extends the previous investigation and examines the formation, development and acoustic consequences of the shock wave. Very complicated bubble-bubble interactions are observed when the shock propagates to the center of the cloud and then produces a rebound of the cloud. The first collapse and rebound, which induce a large volumetric acceleration of the cloud, cause a very large peak in the far-field acoustic noise. The magnitudes of the subsequent peaks in each collapse and rebound cycle may decay rapidly or slowly, depending on the collapse mode of the cloud. After several cycles, the cloud begins to oscillate at its natural frequency. Power spectral density for the far-field noise exhibit the average f^{-n} behavior which is caused by the first few shock-induced acoustic peaks. The index n is found to be between 0.5 and 2 for the cases studied. Some of the spectra have large peaks at the natural frequency of the cloud (see d'Agostino and Brennen 1983 & 1989) and its higher harmonics. These are contributed by the later, regular oscillations of the cloud.

To investigate the strength of the cloud noise and its relationship to the parameters of the flow, the acoustic impulse is calculated for each flow. The normalized impulse is found to be linearly correlated with the normalized maximum total volume of the bubbles, $V_{BMAX}/(0.5D)^3$, in the cloud, where the normalization factor D is the length scale of low pressure perturbation, for example, the diameter of the headform. It is found that $V_{BMAX}/(0.5D)^3$ decreases quasi-linearly with increasing the cavitation number, which ranges from 0.45 to 0.65 in the present study. However, the slope of the dependence changes with the initial void fraction and other parameters, such as D/A_0, the ratio of the length scale of low pressure perturbation to the initial cloud radius. This understanding has important consequences and implications for the scaling of cloud cavitation noise and damage.

2 Basic Equations

Consider a spherical cloud of bubbles surrounded by an unbounded pure liquid at rest at infinity, as shown in figure 1. The pure liquid is assumed incompressible, with a density ρ_L. The relative motion and the mass transfer between the two phases are neglected. It is assumed that the population of bubbles per unit liquid volume, η, within the cloud, is uniform initially and that there is no coalescence or break-up of bubbles; since relative motion is neglected it follows that η

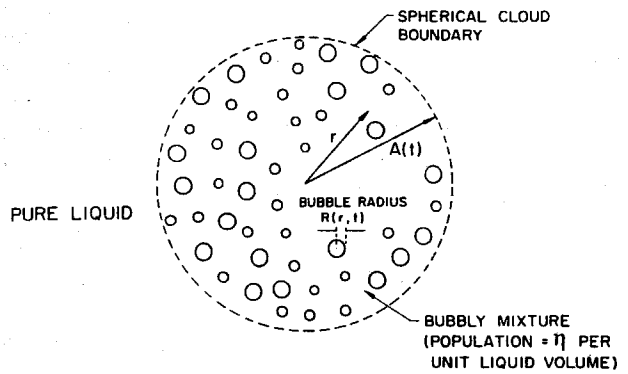

Figure 1: Schematic of a spherical cloud of bubbles

is both constant and uniform within the cloud. The basic equations used are those of d'Agostino *et al.* (1988, 1989) except that all the nonlinear convective terms are retained since these are important in the context of the highly non-linear growth and collapse of the cloud.

The dimensionless forms of the continuity and momentum equations for the one-dimensional spherical bubbly mixture can be written as

$$\frac{1}{r^2}\frac{\partial(r^2u)}{\partial r} = \frac{12\pi\eta R^2}{3+4\pi\eta R^3}\frac{DR}{Dt} \quad ; \quad r \le A(t) \qquad (1)$$

$$\frac{Du}{Dt} = -\frac{1}{6}(3+4\pi\eta R^3)\frac{\partial C_P}{\partial r} \quad ; \quad r \le A(t) \qquad (2)$$

where $\frac{D}{Dt} \equiv \frac{\partial}{\partial t} + u\frac{\partial}{\partial r}$ is the Lagrangian derivative, $u(r,t)$ is the mixture velocity, $R(r,t)$ is the individual bubble radius, $C_P(r,t) = (p(r,t) - p_0)/(\frac{1}{2}\rho_L U^2)$ is the pressure coefficient in the cloud, $p(r,t)$ is the mixture pressure and p_0 is the initial equilibrium pressure in the mixture, $A(t)$ is the radius of the cloud. The bubble population per unit liquid volume, η, is related to the void fraction, α, by $(\frac{4}{3}\pi R^3)\eta = \alpha/(1-\alpha)$. The variables and equations are non-dimensionalized using the initial bubble radius, R_0, a reference flow velocity, U, the time scale, R_0/U, and the dynamic pressure, $\frac{1}{2}\rho_L U^2$. To incorporate the bubble interactive effects, the dynamics of the bubbles are modeled using the Rayleigh-Plesset equation which connects the local mixture pressure coefficient, C_P, to the bubble radius, R:

$$R\frac{D^2R}{Dt^2} = -\frac{1}{2}C_P + \frac{2}{We}[R^{-3k} - R^{-1}] - \frac{3}{2}(\frac{DR}{Dt})^2 + \frac{\sigma}{2}[R^{-3k} - 1] - \frac{4}{Re}\frac{1}{R}\frac{DR}{Dt} \quad ; \quad r \le A(t) \quad (3)$$

where σ, the cavitation number, is an important parameter in the problem.

The above three equations (1), (2), and (3) with appropriate boundary conditions can, in theory, be solved to find the unknown $C_P(r,t)$, $u(r,t)$ and $R(r,t)$ for any bubbly cavitating flow with spherical symmetry. However, the non-linearities in the Rayleigh-Plesset equation and in the Lagrangian derivative, D/Dt, present considerable impediments.

The initial conditions and boundary conditions in the present analysis are as follows. The incompressible liquid flow outside the cloud, $r \ge A(t)$, must have the standard solution of the form:

$$u(r,t) = \frac{C(t)}{r^2} \quad ; \quad r \ge A(t) \qquad (4)$$

$$C_P(r,t) = C_{P\infty}(t) + \frac{2}{r}\frac{dC(t)}{dt} - \frac{C^2(t)}{r^4} \quad ; \quad r \ge A(t) \quad (5)$$

where $C_{P\infty}(t)$ is the known and imposed driving pressure at infinity and $C(t)$ is to be determined. A simple sinusoidal form is chosen for $C_{P\infty}(t)$:

$$C_{P\infty}(t) = \begin{cases} C_{PMIN}\{\cos(\frac{2\pi}{t_G}t) - 1\} & ; 0 < t < t_G \\ 0 & ; t < 0 \text{ and } t > t_G \end{cases} \qquad (6)$$

where C_{PMIN} is the minimum pressure coefficient at infinity and t_G is the dimensionless duration of the low pressure perturbation. Consequently, for a cloud flowing with velocity U past a body of size D, the order of magnitude of t_G will be D/R_0, and C_{PMIN} will be the minimum pressure coefficient of the flow. By combining equations (4) and (5) and substituting $r = A(t)$, we obtain the time-dependent boundary condition at the surface of the cloud:

$$C_P(A(t),t) = C_{P\infty}(t) + \frac{2}{A(t)}\frac{d[A^2(t)u(A(t),t)]}{dt} - u^2(A(t),t) \qquad (7)$$

At the center of cloud, the symmetry of the problem requires

$$u(0,t) = 0 \qquad (8)$$

At time $t \le 0$, it is assumed that the whole flow field is in equilibrium. It is also assumed, for simplicity, that all the bubbles have the same initial radius R_0. Thus we have the following initial conditions:

$$R(r,0) = 1, \quad \frac{DR}{Dt}(r,0) = 0, \quad u(r,0) = 0, \quad C_P(r,0) = 0 \qquad (9)$$

3 Numerical Method

Equations (1) and (2) are rewritten in integral form in terms of the Lagrangian coordinate, (r_0, t), where r_0 is the non-dimensional initial radial position at time $t = 0$. After substituting the boundary conditions, the continuity equation becomes

$$r(r_0,t) = \left[\frac{3}{3+4\pi\eta}\int_0^{r_0}\xi^2(3+4\pi\eta R^3(\xi,t))d\xi\right]^{1/3} \quad (10)$$

$$u(r_0,t) = \frac{\partial r(r_0,t)}{\partial t} = \frac{12\pi\eta}{(3+4\pi\eta)r^2(r_0,t)}\int_0^{r_0}\frac{\partial R(\xi,t)}{\partial t}R^2(\xi,t)\xi^2 d\xi \quad (11)$$

and the momentum equation leads to

$$C_P(r_0,t) = \frac{6}{3+4\pi\eta}\left[\int_{r_0}^{A_0}\frac{f(\xi,t;C_P)-2r(\xi,t)u^2(\xi,t)}{r^4(\xi,t)}\xi^2 d\xi\right] + \frac{2f(A_0,t)}{r(A_0,t)} - u^2(A_0,t) + C_{P\infty}(t) \quad (12)$$

where

$$f(\xi,t;C_P) = \frac{12\pi\eta}{3+4\pi\eta}\int_0^{\xi}\left\{\frac{2}{We}[R^{1-3k}(\zeta,t)-1] - \frac{4}{Re}\frac{\partial R(\zeta,t)}{\partial t} + \frac{\sigma}{2}R(\zeta,t)[R^{-3k}(\zeta,t)-1] + \frac{1}{2}R(\zeta,t)[(\frac{\partial R(\zeta,t)}{\partial t})^2 - C_P]\right\}\zeta^2 d\zeta \quad (13)$$

A complete integration time step therefore proceeds as follows.

1) $R(r_0, t+\Delta t)$ and $\frac{\partial R(r_0,t+\Delta t)}{\partial t}$ are calculated using Taylor's series expansion of the solution at the previous time step, $R(r_0,t)$, $\frac{\partial R(r_0,t)}{\partial t}$ and $\frac{\partial^2 R(r_0,t)}{\partial t^2}$.

2) With $R(r_0,t+\Delta t)$ and $\frac{\partial R(r_0,t+\Delta t)}{\partial t}$, equations (10) and (11) can be integrated to obtain $r(r_0,t+\Delta t)$ and $u(r_0,t+\Delta t)$.

3) With the results of steps 2 and 3, we can use equation (12) to find $C_P(r_0,t+\Delta t)$. Then the Rayleigh-Plesset equation (3) can be used to find $\frac{\partial^2 R(r_0,t+\Delta t)}{\partial t^2}$.

4) Proceed to next time step.

Under-relaxation must be used in the iteration step 3 to achieve convergence. The rate of convergence is found to be dependent on the initial void fraction α_0; the larger α_0, the slower the convergence. The program automatically adjusts the interval of each time step to ensure that the fractional change in bubble radius between any two consecutive times does not exceed some specific value (typically, 5%). This is essential for time marching through a violent bubble collapse.

4 Results and Discussion

The flow condition in the present study is chosen as follows. A cloud of nuclei, composed of air bubbles of initial radius R_0=100 μm in water at 20°C, flows with velocity U=10 m/sec. The computation is performed at different combinations of the following parameters: initial void fraction, α_0, of 0.03%, 0.3%, and 3%; cavitation number, σ, of 0.45, 0.55, and 0.65; the minimum pressure coefficient, C_{PMIN}, of -0.75; the non-dimensional cloud radius, A_0, of 32, 100, and 312; the non-dimensional duration of the low pressure perturbation, t_G, of 50, 100, 500, and 1000. These ranges of values of A_0 and t_G correspond to the ratio of the length scale of the low pressure perturbation to the initial radius of the cloud, D/A_0, of 0.5 → 31.25. The Reynolds number, $Re = UR_0\rho_L/\mu_E$, based on the reference flow velocity, initial bubble radius, and the liquid density, is 0.05 in all the cases presented. Here we have used the the effective liquid viscosity, μ_E, in place of actual liquid viscosity to incorporate the various bubble damping mechanisms (see Chapman and Plesset, 1971).

The computational results show that the characteristics of the growth of the cloud are similar to those of a single bubble and that all bubbles in the cloud grow almost in phase. However, the bubbles in the interior are shielded to some extent by the bubbles on the surface of the cloud and so grow more slowly and have a smaller maximum size, as shown in figures 2, 3 and 4.

At large void fraction, due to the strong influence of neighboring bubbles, bubble growth is severely restrained. Therefore, the distribution of bubble growth rate inside the cloud is rather uniform and all bubbles away from the near-surface region grow to about the same maximum size, as shown in figures 2 and 3.

Figure 4 presents a case with small void fraction (α_0 = 0.03%) and large duration of the low pressure perturbation (t_G = 1000 or D/A_0 = 10). In this case the surface bubbles can grow more freely for a long time. Although the shielding effect is weaker than in the case of figure 2, the closer the bubbles are to the center of the cloud, the more slowly they grow; therefore the smallest bubbles occur near the center of the cloud. The maximum size of the bubbles on the surface

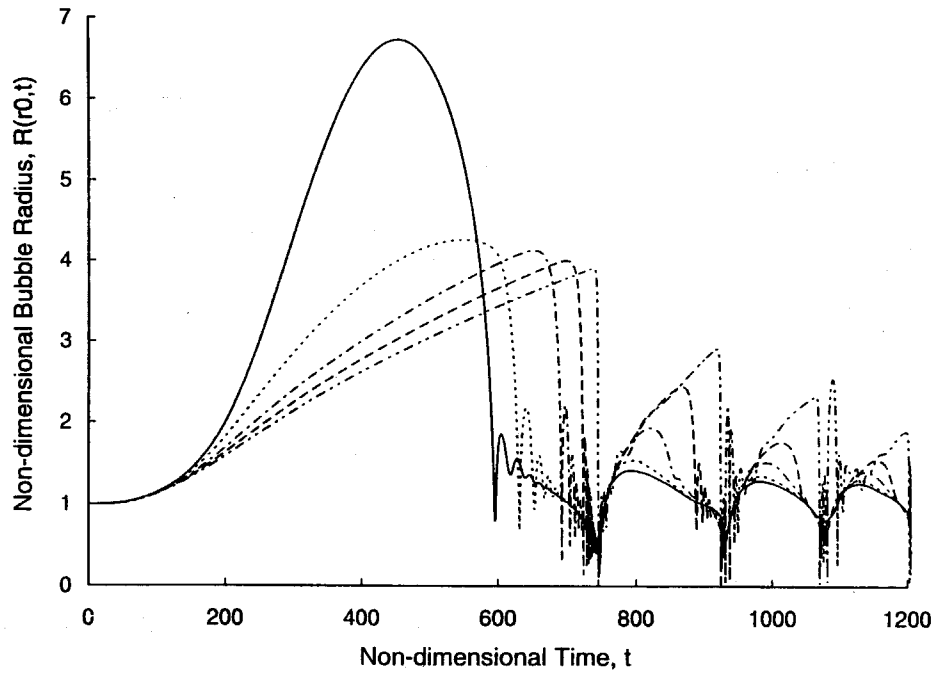

Figure 2: The time history of the dimensionless bubble size at five different positions in the cloud; $r_0 = 0$ (dash-dot-dot line), $r_0 = 0.5A_0$ (dashed line), $r_0 = 0.7A_0$ (dash-dot line), $r_0 = 0.9A_0$ (dotted line), and $r_0 = A_0$ (solid line). Parameters used are σ=0.45, C_{PMIN}=-0.75, α_0=3%, A_0=100, and the ratio of the low pressure perturbation length to initial cloud radius, $D/A_0 = 5$, which corresponds to the duration of the low pressure perturbation, t_G= 500.

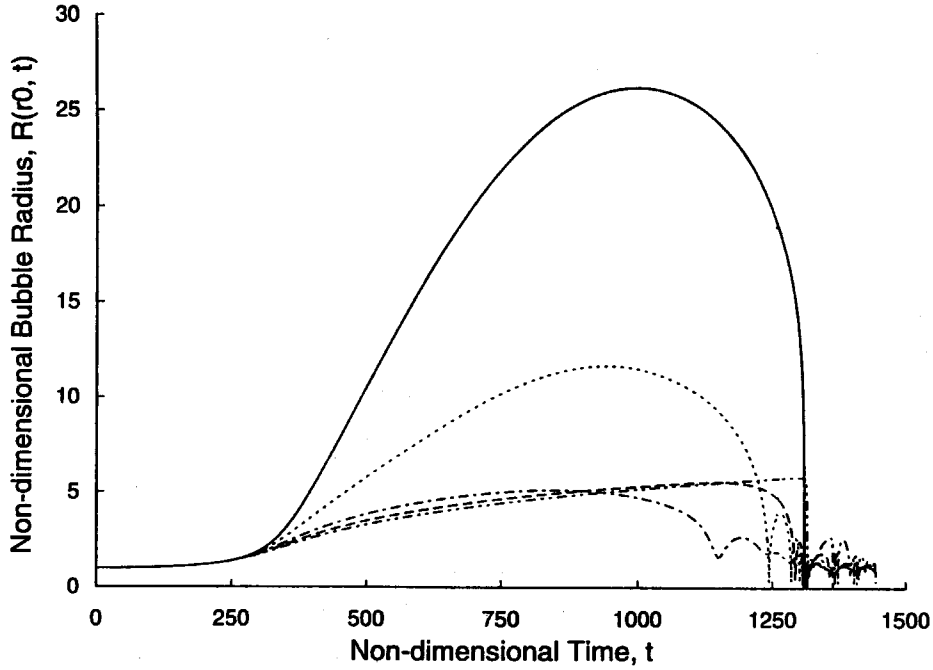

Figure 3: The time history of the dimensionless bubble size at five different positions in the cloud; $r_0 = 0$ (dash-dot-dot line), $r_0 = 0.5A_0$ (dashed line), $r_0 = 0.7A_0$ (dash-dot line), $r_0 = 0.9A_0$ (dotted line), and $r_0 = A_0$ (solid line). Parameters used are $\alpha_0 = 0.3\%$, $D/A_0 = 10$ or $t_G = 1000$. Other parameters as in figure 2.

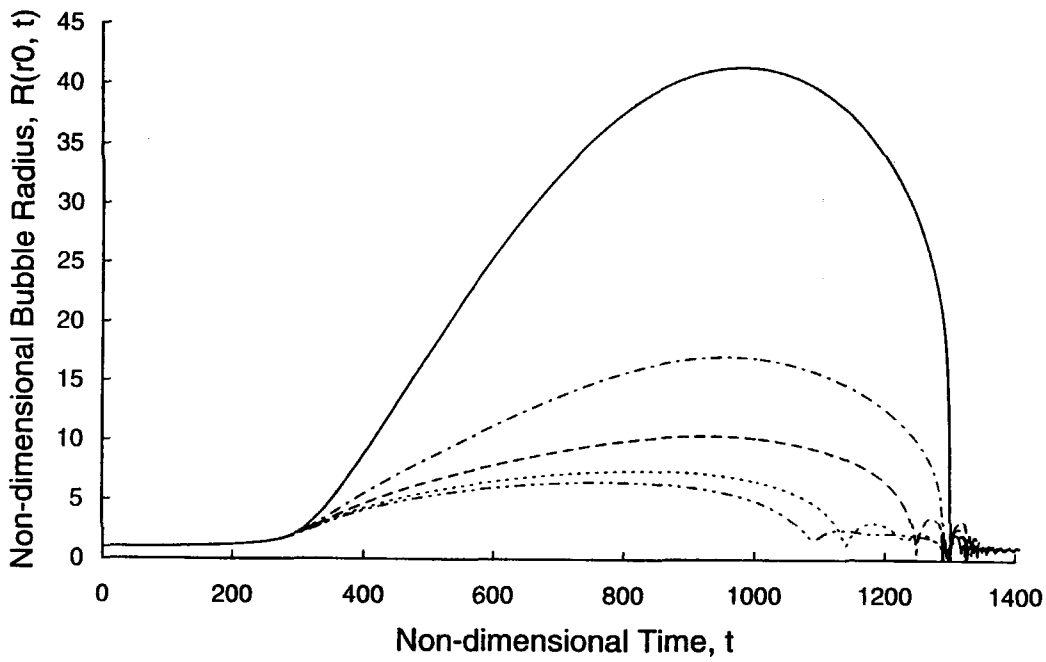

Figure 4: The time history of the dimensionless bubble size at five different positions in the cloud; $r_0 = 0$ (dash-dot-dot line), $r_0 = 0.3A_0$ (dotted line), $r_0 = 0.5A_0$ (dashed line), $r_0 = 0.7A_0$ (dash-dot line), and $r_0 = A_0$ (solid line). Parameters used are $\alpha_0 = 0.03\%$, $D/A_0 = 10$ or $t_G = 1000$. Other parameters as in figure 2.

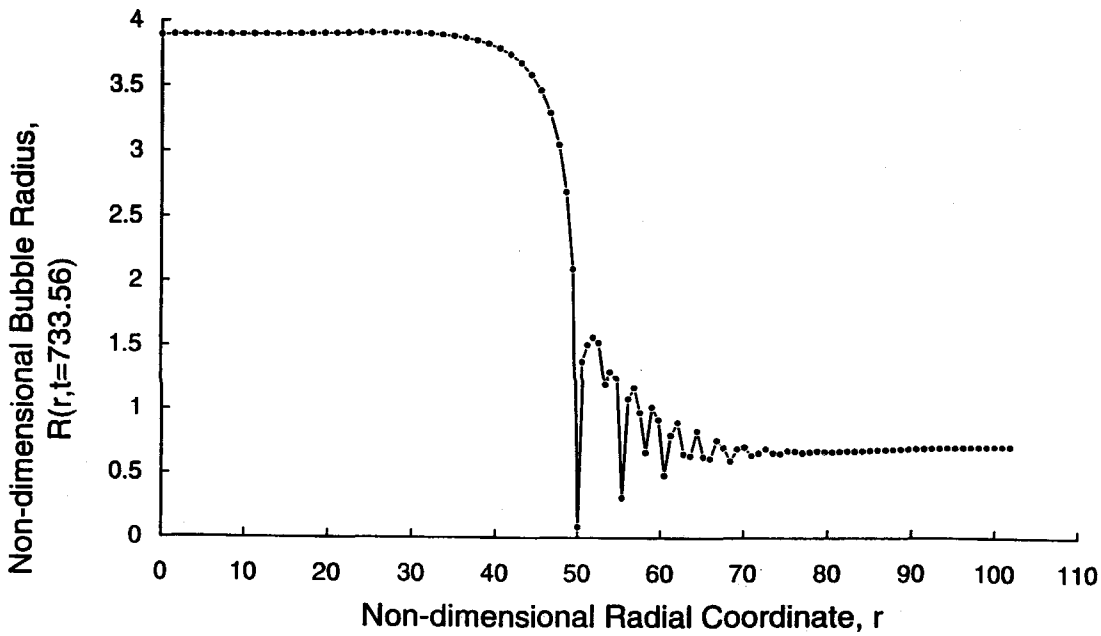

Figure 5: The dimensionless bubble size distribution in the cloud as a function of the dimensionless cloud radius at the dimensionless time, $t = 733.56$. Parameters as in figure 2.

can be up to an order of magnitude larger than those of the bubbles near the center. These radial gradients in the bubble growth rate and bubble maximum size result in the following differences in the cloud collapse mechanisms. There appear to be three collapse scenarios, depending on the initial void fraction, α_0, and the ratio of the length scale of the low pressure perturbation to initial cloud radius, D/A_0.

If the void fraction is sufficiently large and the size ratio, D/A_0, is of order one, the recovery of the ambient pressure causes bubbles on the surface of the cloud to collapse first. The accelerations induced by the collapse of the surface bubbles promote the collapse of the neighboring bubbles and then the collapse spreads inward, as shown in figure 2. The shielding effect causes the bubbles in the core region (approximately 0.7 cloud radius) to continue to grow even after the surface layer bubbles have totally collapsed. As a result of the collapse of the surface layer, a shock wave develops and propagates inward through the bubbly mixture. Figure 5 shows the structure of the shock wave, which is similar to to that of the steady planar shocks analyzed by Noordij and van Wijngaarden (1974). The shock wave strengthens not only because of the geometric effect of an inwardly propagating spherical shock but also because of the coupling of the single bubble dynamics with the global dynamics of the flow through the pressure and velocity fields. A very large pressure pulse can be generated when the shock passes bubbles and causes them collapse, as shown in figure 6. Very complicated bubble-bubble interactions are observed in figures 2 when the focusing shock reaches the center of the cloud, produces very high pressures, and then causes a rebound of the cloud.

On the other hand, if the void fraction is small and the duration of the low pressure perturbation is large (D/A_0 large), as in the case of figure 4, the bubbles near the center of the cloud reach the smallest maximum size and tend to collapse first. As a result, the collapse spreads outward from the center and no shock-enhancing process develops. The resulting acoustic impulse is much smaller than that of the previous mode of collapse.

There is an intermediate type of collapse illustrated in figure 3. The initial void fraction, $\alpha_0 = 0.3\%$, is an intermediate value. The collapse starts at mid-radius and spreads inward and outward at the same time. Examining the distribution of the bubble growth rate in the cloud, it is found that, even for an initial void fraction of 0.3%, the shielding effect is still strong in the core region of the cloud. The growth of bubbles in this core therefore continues after bubbles at larger radii have begun to collapse. The outward moving collapse front tends to cancel the inward acceleration of the flow caused by the collapse of the bubbles on the surface of the cloud. The inward moving collapse front is similar to the shock wave described earlier. However, the shock-focusing effect is weaker due to the reduced "effective collapse size" of the cloud.

A typical time history of the radius of the cloud is shown in figure 7. Note that, unlike single bubbles, the cloud radius, $A(t)$, only decreases to a size marginally smaller than its equilibrium size during the collapse process. But each volumetric rebound will cause an acoustic peak in the far field, as shown in figure 8. The normalized acoustic noise, p_a, can be calculated from the volumetric acceleration of the cloud and is given by

$$p_a(t) = \frac{2R_0}{D}\left[A^2(t)\frac{d^2A(t)}{dt^2} + 2A(t)(\frac{dA(t)}{dt})^2\right] \quad (14)$$

where the length scale of normalization has been chosen as the length of the low pressure region, D. The non-dimensional power spectral density of the acoustic noise in figure 8 is shown as a function of dimensionless frequency in figure 9. This spectrum exhibits the f^{-2} behavior for the frequency range below 0.25 ($25kHz$) which is typical of cavitation noise (see, for example, Arakeri and Shangumanathan 1985, Blake *et al.* 1977). It has been found that spectra of other cases also show the average f^{-n} behavior and the index n is in the range of $0.5 \rightarrow 2$. If we let the computation progress further in time, the magnitude of the cloud oscillation will further decay and the cloud will begin to oscillate in a regular way, as shown in figure 10. This regular oscillation contributes large peaks in the spectrum at the natural frequency of the cloud (see d'Agostino and Brennen 1983 & 1989) and at higher harmonics, as shown in figure 11.

A good measure of the strength of the collapse noise is the acoustic impulse, I, defined as the area under the pulse or

$$I = \int_{t_1}^{t_2} p_a(t)dt \quad (15)$$

where t_1 and t_2 are times before and after the pulse at which p_a is zero. The impulses from calculations using a wide variety of parameter choices (45 permutations) are found to be linearly correlated with the maximum total volume of the bubbles in the cloud normalized by the length of the low pressure perturbation, $V_{BMAX}/(0.5D)^3$, as shown in figure 12. To complete the picture, figure 13 demonstrates that $V_{BMAX}/(0.5D)^3$ decreases quasi-linearly with increasing cavitation number and with increase in the initial

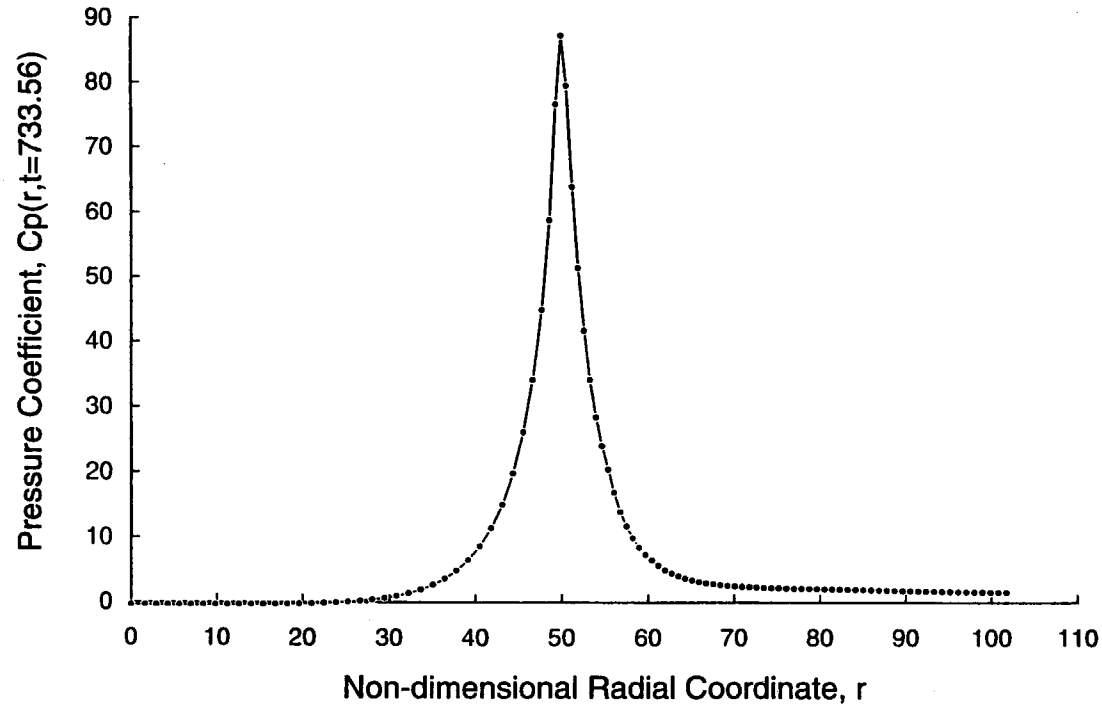

Figure 6: The pressure coefficient distribution in the cloud as a function of the dimensionless cloud radius at dimensionless time, $t = 733.56$. Parameters as in figure 2.

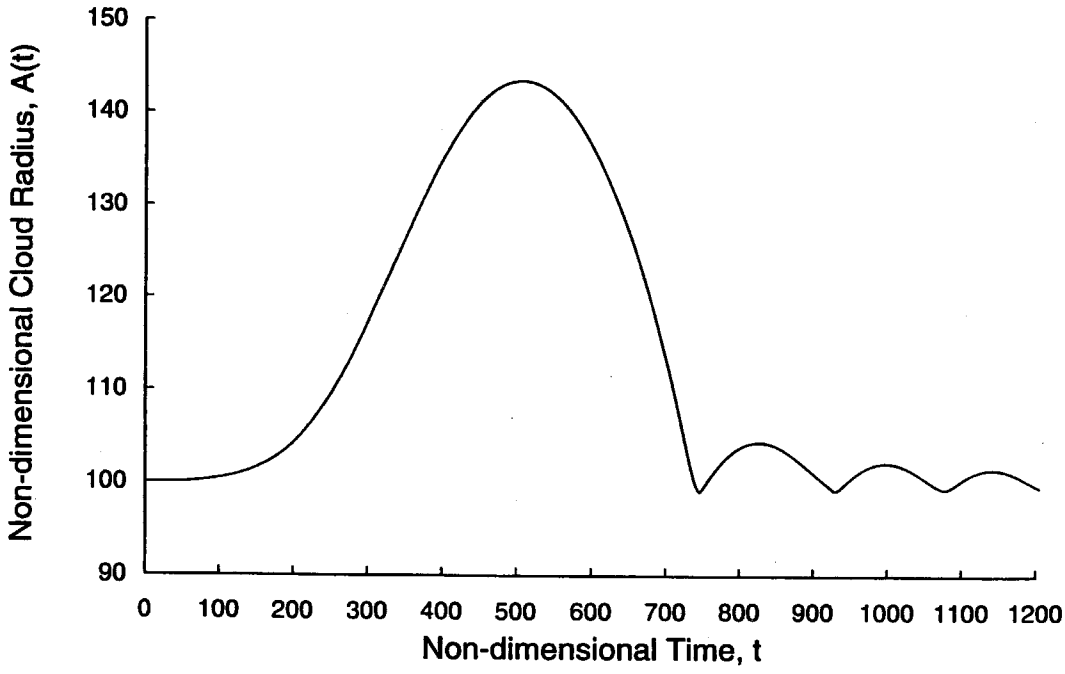

Figure 7: The time history of the dimensionless cloud radius. Parameters as in figure 2.

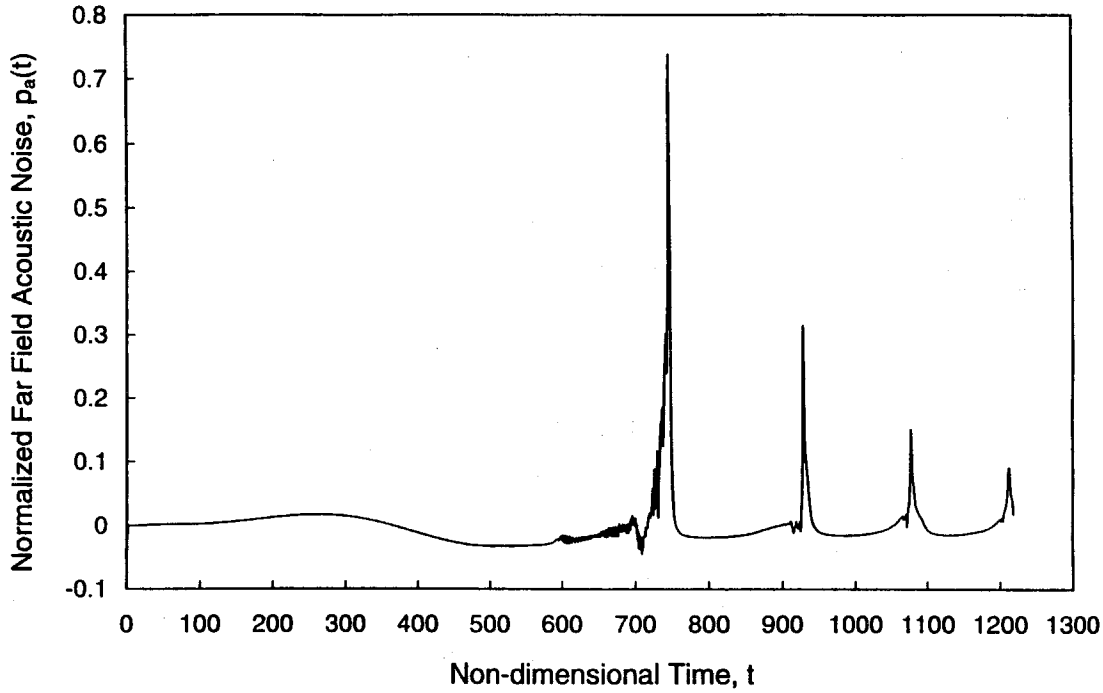

Figure 8: The time history of the far field cloud acoustic noise calculated from the data of figure 7.

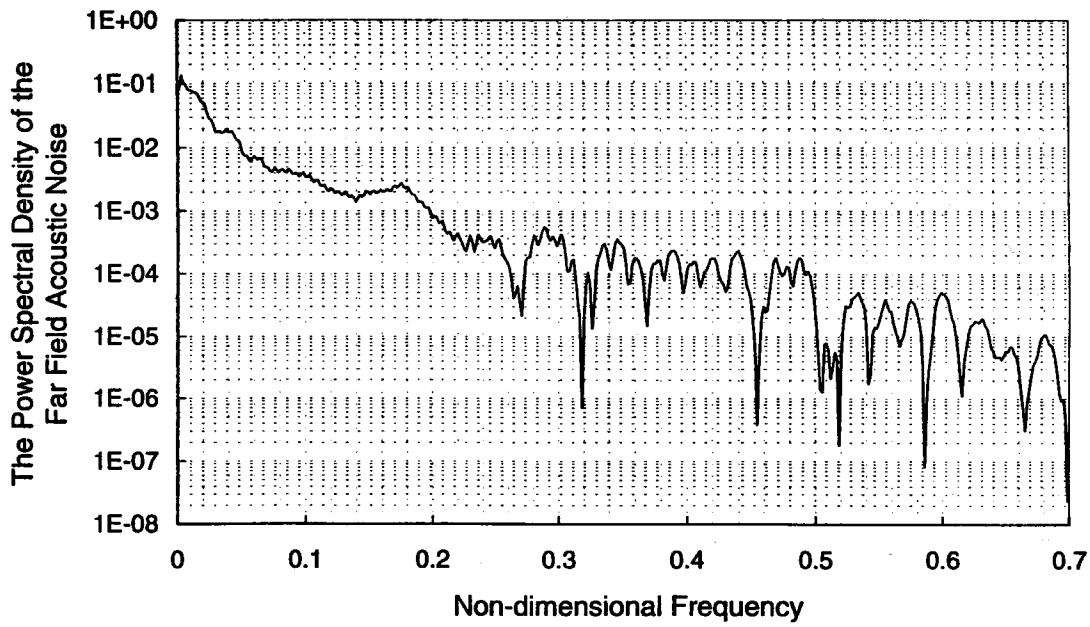

Figure 9: The non-dimensional power spectral density of the far field acoustic noise in figure 8.

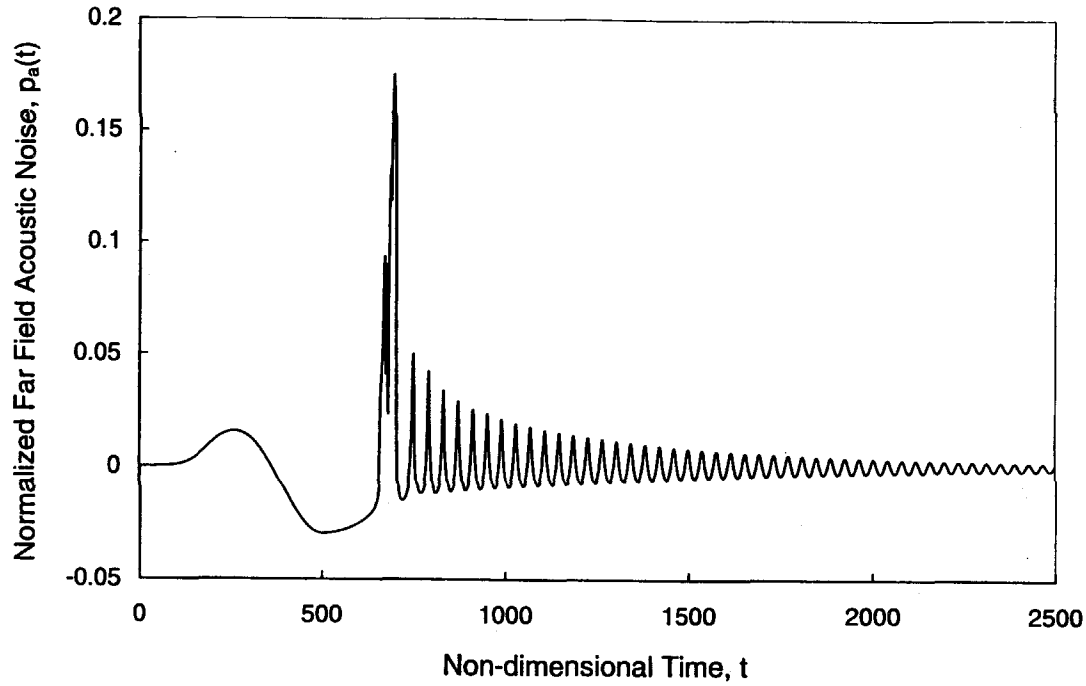

Figure 10: The time history of the far field cloud acoustic noise for the case of $\alpha_0 = 0.3\%$. Other parameters as in figure 2.

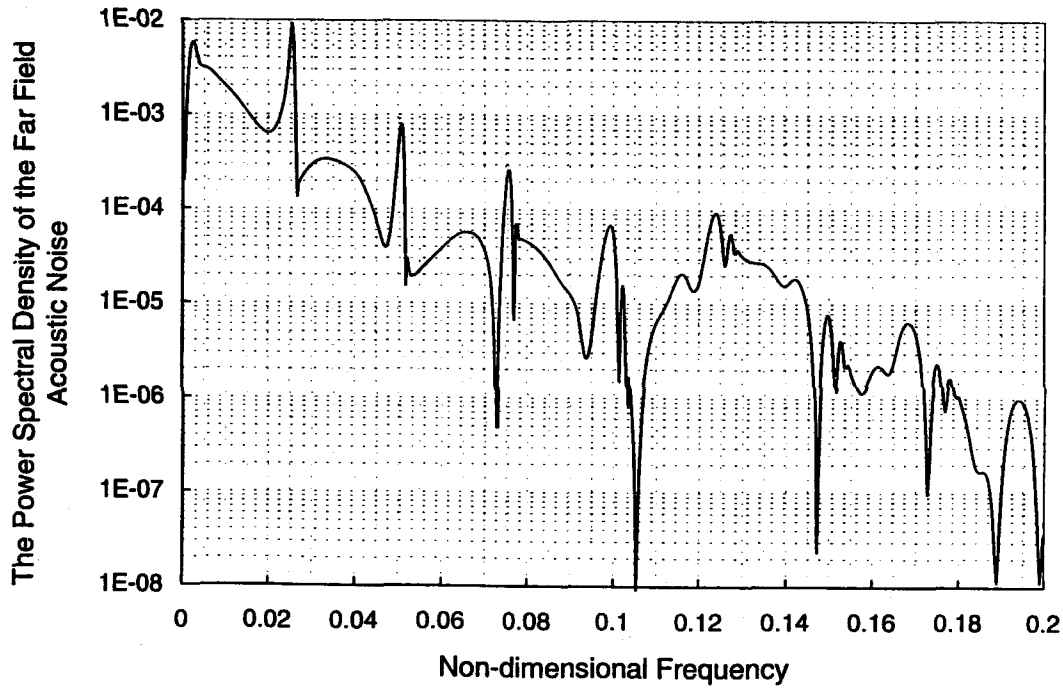

Figure 11: The non-dimensional power spectral density of the far field acoustic noise in figure 10 as a function of dimensionless frequency. The lowest cloud natural frequency in this case is 0.026. The peak located at 0.002 corresponds to the driving frequency of the low pressure perturbation.

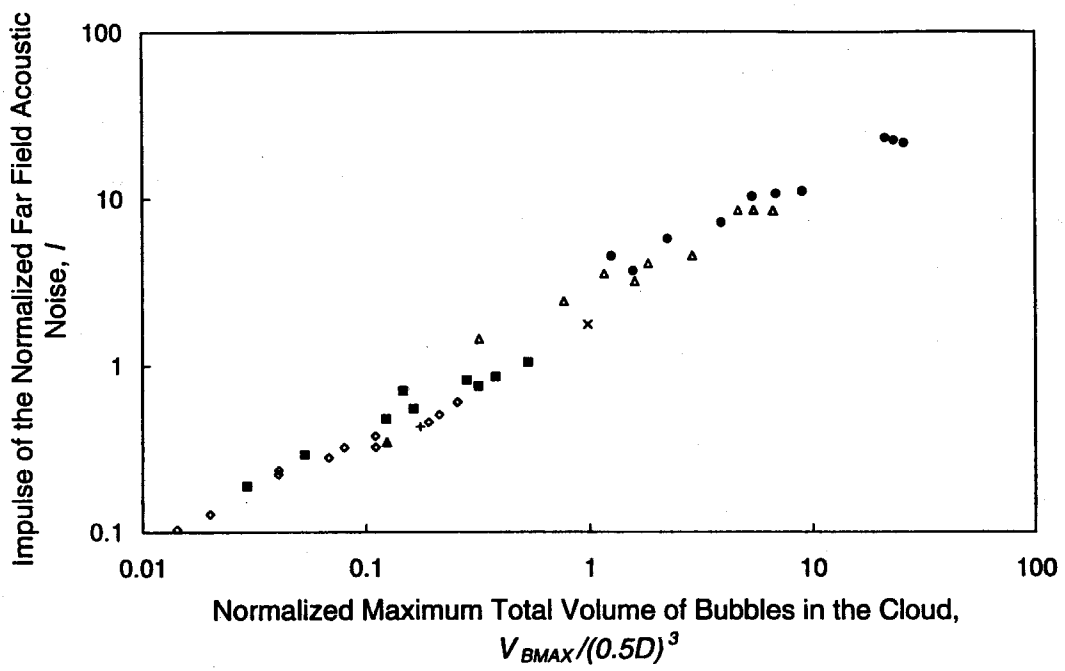

Figure 12: The impulse of the normalized far field acoustic noise correlated with the normalized maximum total volume of bubbles in the cloud at different ratio of the length scale of the low pressure perturbation to the initial radius of the cloud, D/A_0, (31.25 = solid $\triangle$, 15.625 = +, 10 = $\diamond$, 5 = solid $\square$, 3.125 = $\times$, 1 = $\triangle$, 0.5 = $\bullet$).

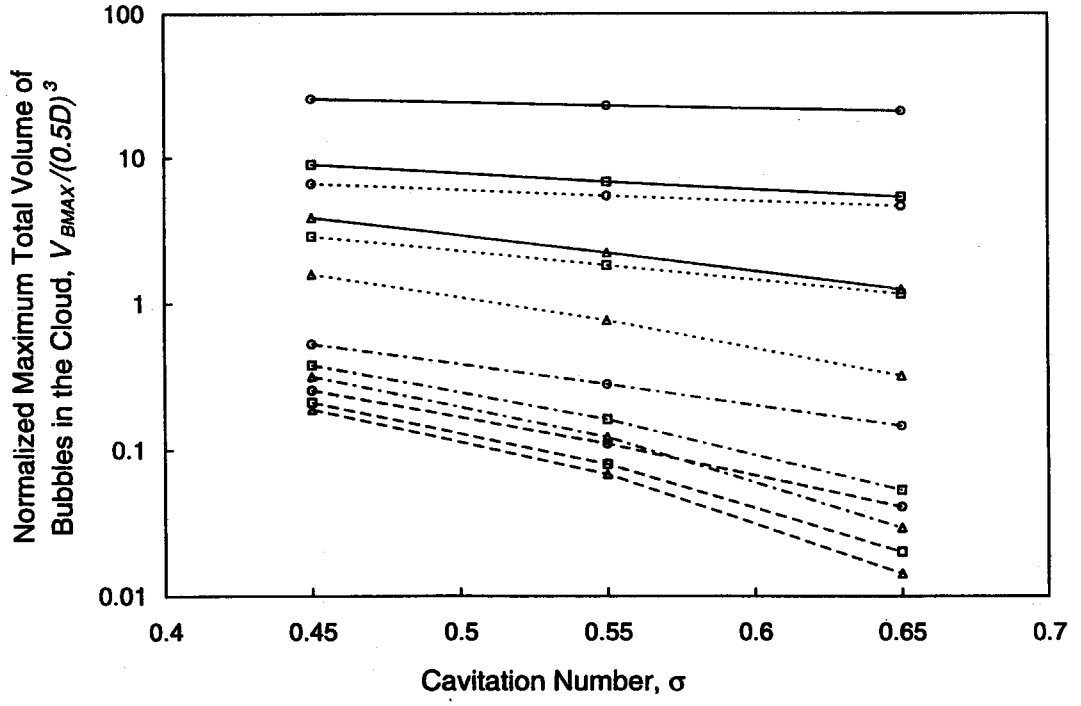

Figure 13: The normalized maximum total volume of bubbles in the cloud as a function of cavitation number. Data is shown for four different size ratios D/A_0 (0.5 = solid lines, 1.0 = dotted lines, 5.0 = dash-dot lines, 10 = dashed lines) and three initial void fractions, α_0, (3% = $\circ$, 0.3% = $\square$, 0.03% = $\triangle$). Other parameters as in figure 2.

void fraction, α_0. However, the slope of the dependence changes with α_0 and D/A_0. The smaller α_0, the weaker the shielding effect, the larger the slope.

5 Conclusions

This paper has presented numerical calculations of the non-linear growth and collapse of a spherical cloud of cavitation bubbles. The continuum equations for the flow are coupled with the Rayleigh-Plesset dynamics for the bubbles. The characteristics dynamics are shown to be strongly dependent on the parameter $\alpha_0(1-\alpha_0)A_0^2/R_0^2$ where α_0 is the initial void fraction, A_0 is the initial cloud radius and R_0 is the initial bubble radius. Three modes of collapse have been identified. At large values of this parameter, the collapse involves the formation of an inward propagating shock wave which initially forms at the surface of the cloud. This shock dominates this first mode of collapse and strengthens rapidly due to geometric focusing and the coupling of the bubble dynamics with the flow. In this mode, a large pulse in the far-field noise is produced by the arrival of the shock at the cloud center. Moreover, there are further but weaker shocks which arrive at the center and thus produce a train of acoustic impulses which, eventually, leads into a regular oscillation of the cloud at the first cloud natural frequency.

A different mode of collapse occurs at low values of $\alpha_0(1-\alpha_0)A_0^2/R_0^2$. Then the shielding effects of the outer bubbles causes the bubbles in the core of the cloud to grow to a smaller maximum size and to collapse first. This creates an outward moving collapse front and a very different mode of collapse than occurs at high $\alpha_0(1-\alpha_0)A_0^2/R_0^2$. At intermediate values, we observe cases where collapse first occurs at an intermediate radius and collapse fronts then propagate both outward and inward from this location.

We have also correlated the far-field acoustic impulse produced in all these cases with the parameters of the problem. It was found that the impulse is strongly correlated with the maximum total volume of bubbles in the cloud. Moreover, this total volume decreases with increasing cavitation number and with increasing void fraction. It also varies with D/A_0 where D is the typical length of the low pressure perturbation.

Acknowledgments

The authors are very grateful for the support for this research provided by the Office of Naval Research under Contract N00014-91-J-1295.

References

[1] Arakeri, V.H. and Shangumanathan, V. (1985). On the evidence for the effect of bubble interference on cavitation noise. *J. Fluid Mech.*, **159**, 131-150.

[2] Bark, G. and Berlekom, W.B. (1978). Experimental investigations of cavitation noise. *Proc. 12th ONR Symp. on Naval Hydrodynamics*, 470-493.

[3] Bark, G. (1985). Developments of distortions in sheet cavitation on hydrofoils. *Proc. ASME Int. Symp. on Jets and Cavities*, 470-493.

[4] Blake, W.K., Wolpert, M.J. and Geib, F.E. (1977). Cavitation noise and inception as influenced by boundary-layer development on a hydrofoil. *J. Fluid Mech.*, **80**, 617-640.

[5] Chapman, R.B. and Plesset, M.S. (1971). Thermal effects in the free oscillation of gas bubbles. *ASME J. Basic Eng.*, **93**, 373-376.

[6] d'Agostino, L. and Brennen, C.E. (1983). On the acoustical dynamics of bubble clouds. *ASME Cavitation and Multiphase Flow Forum*, 72-75.

[7] d'Agostino, L. and Brennen, C.E., Acosta, A.J. (1988). Linearized dynamics of two-dimensional bubbly and cavitating flows over slender surfaces. *J. Fluid Mech.*, **192**, 485-509.

[8] d'Agostino, L. and Brennen, C.E. (1988). Acoustical absorption and scattering cross-sections of spherical bubble clouds. *J. Acoust. Soc. Am.*, **84**, 2126-2134.

[9] d'Agostino, L. and Brennen, C.E. (1989). Linearized dynamics of spherical bubble clouds. *J. Fluid Mech.*, **199**, 155-176.

[10] Franc, J.P. and Michel, J.M. (1988). Unsteady attached cavitation on an oscillating hydrofoil. *J. Fluid Mech.*, **193**, 171-189.

[11] Hanson, I., Kedrinskii, V.K. and Mørch, K.A. (1981). On the dynamics of cavity clusters. *J. Appl. Phys.*, **15**, 1725-1734.

[12] Kubota, A., Kato, H., Yamaguchi, H. and Maeda, M. (1989). Unsteady structure measurement of cloud cavitation on a foil section using conditional sampling. *J. Fluids Eng.*, **111**, 204-210.

[13] Kumar, S. and Brennen, C.E. (1991). Non-linear effects in the dynamics of clouds of bubbles. *J. Acoust. Soc. Am.*, **89**, 707-714.

[14] Kumar, S. and Brennen, C.E. (1992). Harmonic cascading in bubble clouds. *Proc. Int. Symp. on Propulsors and Cavitation, Hamburg*, 171-179.

[15] Kumar, S. and Brennen, C.E. (1993). Some nonlinear interactive effects in bubbly cavitating clouds. *J. Fluid Mech.*, **253**, 565-591.

[16] Mørch, K.A. (1980). On the collapse of cavity cluster in flow cavitation. *Proc. First Int. Conf. on Cavitation and Inhomogeneities in Underwater Acoustics, Springer Series in Electrophysics*, **4**, 95-100.

[17] Mørch, K.A. (1981). Cavity cluster dynamics and cavitation erosion. *Proc. ASME Cavitation and Polyphase Flow Forum*, 1-10.

[18] Noordij, L. and van Wijngaarden, L. (1974). Relaxation effects, caused by relative motion, on shock waves in gas-bubble/liquid mixtures. *J. Fluid Mech.*, **66**, 115-143.

[19] Reisman, G.E., McKenney, E.A. and Brennen, C.E. (1994). Cloud cavitation on an oscillating hydrofoil. *Proc. 20th ONR Symp. on Naval Hydrodynamics*, 78-89.

[20] Shen, Y. and Peterson, F.B. (1978). Unsteady cavitation on an oscillating hydrofoil. *Proc. 12th ONR Symp. on Naval Hydrodynamics.*, 362-384.

[21] Soyama, H., Kato, H. and Oba, R. (1992). Cavitation observations of severely erosive vortex cavitation arising in a centrifugal pump. *Proc. Third I.Mech.E. Int. Conf. on Cavitation*, 103-110.

[22] Wang, Y.-C. and Brennen, C.E. (1994). Shock wave development on the collapse of a cloud of bubbles. *Cavitation and Multiphase Flow Forum*, FED vol. **194**, 15-19.